Unmixing Multitemporal Hyperspectral Images Accounting for Smooth and Abrupt Variations

Pierre-Antoine Thouvenin, Nicolas Dobigeon and Jean-Yves Tourneret

University of Toulouse, IRIT/INP-ENSEEIHT

EUSIPCO 2017, Kos, Greece

September 1, 2017

Work funded by the Direction Générale de l'Armement, French Ministry of Defense.

A brief introduction to hyperspectral unmixing

- Airborne/spaceborne hyperspectral (HS) images: high spectral resolution (10 nm), comparatively lower spatial resolution (20 m $\times$ 20 m);
- Observations: mixture of several spectra corresponding to distinct materials (*endmembers*);
- Endmembers present in unknown proportions in each pixel (*abundance*, quantitative spatial mapping).

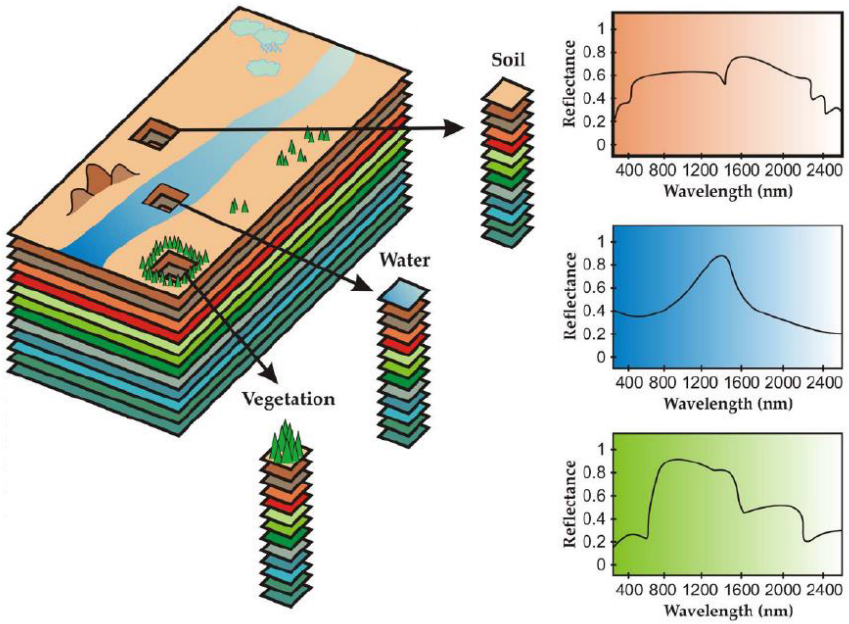

Figure 1: Hyperspectral unmixing: an illustration (taken from [1]).

Linear mixture model

Linear mixture model

Traditionally, observations are represented by a linear combination of the unknown endmembers [1]

$$\forall n \in \{1, \dots N\}, \quad \mathbf{y}_n = \sum_{r=1}^{R} a_{rn}\mathbf{m}_r + \mathbf{b}_n \tag{1}$$

$$\mathbf{Y} = \mathbf{MA} + \mathbf{B} \tag{2}$$

Constraints (physical interpretability)

$$\mathbf{A} \succeq \mathbf{0}_{R,N}, \quad \mathbf{A}^T\mathbf{1}_R = \mathbf{1}_N, \quad \mathbf{M} \succeq \mathbf{0}_{L,R} \tag{3}$$

- Several models are available in the literature to capture more complex interations between light and matter [2, 3, 4, 5] (e.g. multiple reflections).
- A given material is assumed to be fully characterized by a single signature.

Endmember variability

- Endmembers possibly affected by local environmental factors, varying acquisition conditions: spectral variability;
- Spatial variability: significant source of errors when estimating the abundance coefficients;
- Error propagation within unsupervised unmixing procedures $\Rightarrow$ need for appropriate models.

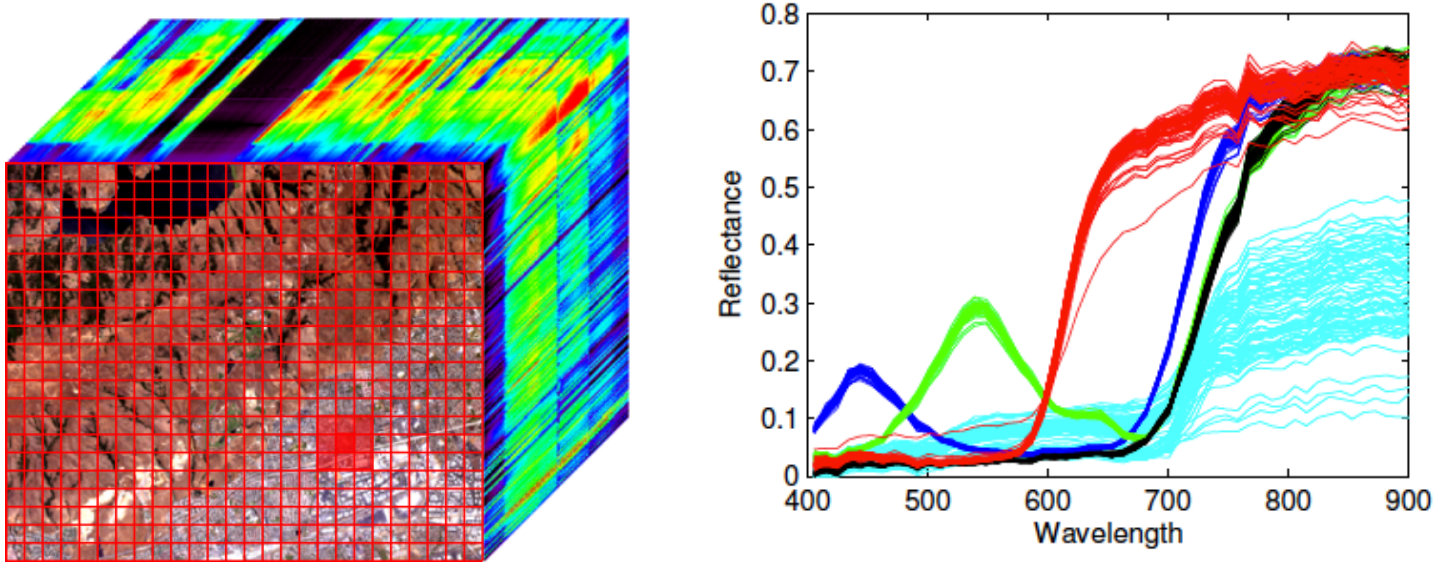

(a) Spatial variability (inter-pixel) (b) Endmember variability[1]

Figure 2: Endmember spatial variability: an illustration.

[1] P. Gader, A. Zare, R. Close, J. Aitken, G. Tuell, MUUFL Gulfport Hyperspectral and LiDAR Airborne Data Set, University of Florida, Gainesville, FL, Tech. Rep. REP-2013-570, Oct. 2013.

Temporal endmember variability

- Variability: a prominent issue when considering multi-temporal hyperspectral (MTHS) images
  - ▷ varying acquisition conditions;
  - ▷ natural evolution of the scene (e.g. water, vegetation).

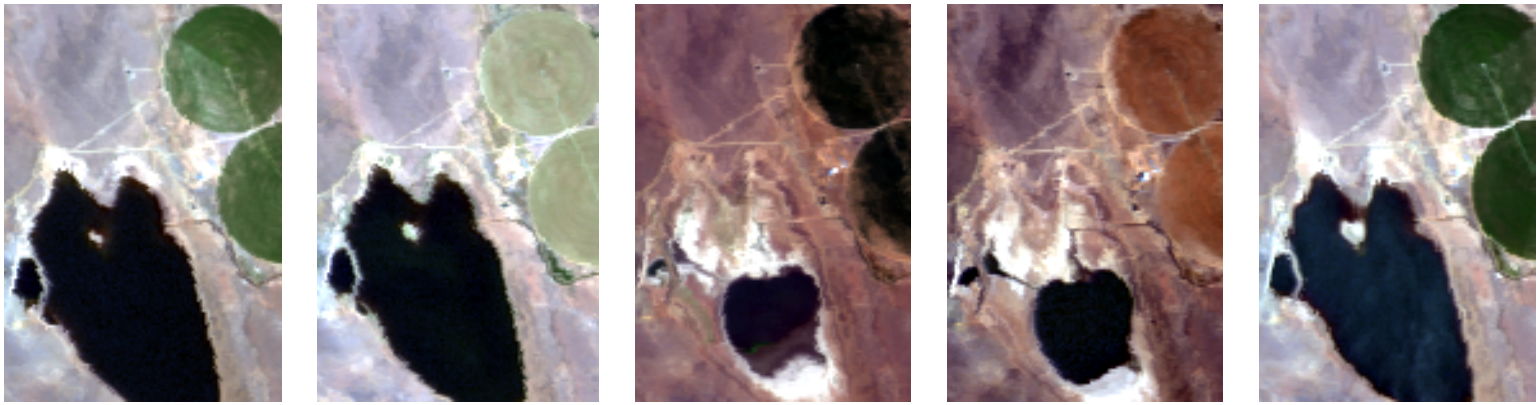

(a) 10/04/14 (b) 02/06/14 (c) 19/09/14 (d) 17/11/14 (e) 29/04/15

Figure 3: An example of a sequence of hyperspectral images, acquired at different time instants.

Variability accounting methods

Essentially two modeling paradigms

- Automated endmember bundles (AEB) [6, 7, 8]
  - ▷ unmixing relies on spectral libraries, either extracted from the data or *a priori* available.
- Normal compositional model (NCM) [9, 10], Beta compositional model (BCM) [11]
  - ▷ endmembers modeled as realizations of random vectors.

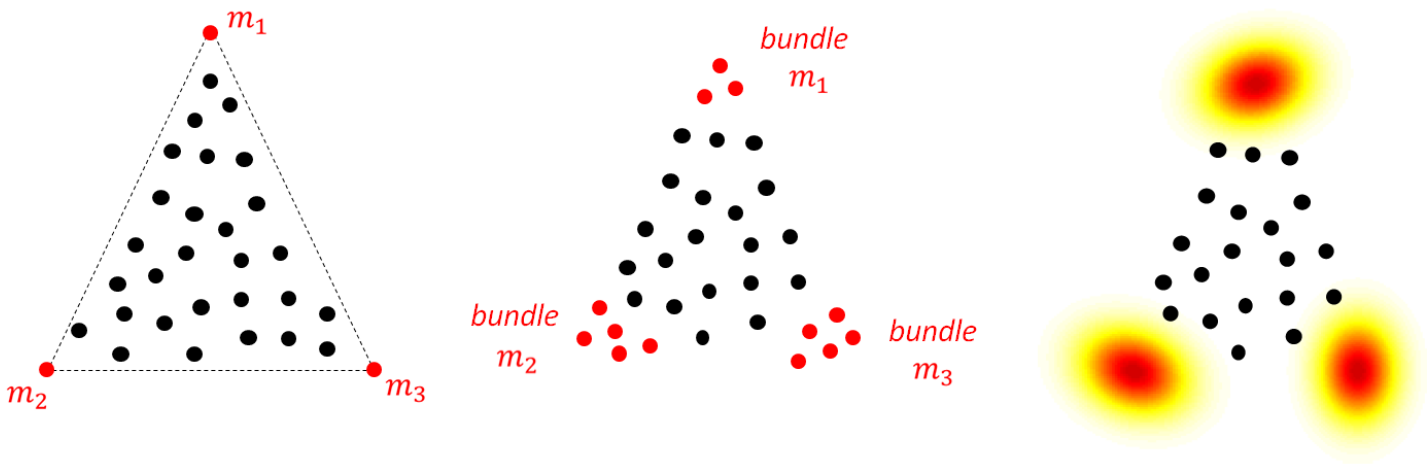

Figure 4: Different representations of endmember variability within the simplex enclosing the data (image taken from [10]).

Overview

Context and motivations

Observations:

- some of the observed materials present moderate variations across time (man-made constructions, ...);
- signatures corresponding to materials present in the different images
  - ▷ realizations of reference endmembers $\Rightarrow$ variability;
- abrupt variations may occur (e.g., when water or vegetation are present in the observed scene)
  - ▷ new material or a sensor default $\Rightarrow$ abrupt spectral changes $\Rightarrow$ outlier w.r.t. the commonly shared materials.

Proposed approach:

- ▶ unmix a reference HS image to obtain an initial estimate for the endmembers;
- ▶ use / refine this result when unmixing the remaining images.

Model:

- ▶ represent smooth endmember variations as temporal variability;
- ▶ interpret abrupt spectral variations in terms of outliers.

Model

Model and constraints

$$\mathbf{Y}_t = (\mathbf{M} + \mathbf{dM}_t)\mathbf{A}_t + \mathbf{X}_t + \mathbf{B}_t \tag{4}$$

$$\begin{aligned} &\mathbf{A}_t \succeq \mathbf{0}_{R,N},\ \mathbf{A}_t^{\mathsf{T}}\mathbf{1}_R = \mathbf{1}_N,\ \forall t \in \{1,\dots,T\} \\ &\mathbf{M} \succeq \mathbf{0}_{L,R},\ \mathbf{M} + \mathbf{dM}_t \succeq \mathbf{0}_{L,R},\ \mathbf{X}_t \succeq \mathbf{0}_{L,N} \end{aligned} \tag{5}$$

Likelihood function

$$p(\underline{\mathbf{Y}} \mid \Theta) \propto \prod_{t=1}^{T} (\sigma_t^2)^{-NL/2} \exp\left(-\frac{1}{2\sigma_t^2} \|\mathbf{Y}_t - (\mathbf{M} + \mathbf{dM}_t)\mathbf{A}_t - \mathbf{X}_t\|_{\mathrm{F}}^2\right)$$

where $\Theta = \{\mathbf{M}, \mathbf{d}\underline{\mathbf{M}}, \underline{\mathbf{A}}, \underline{\mathbf{X}}, \mathbf{Z}, \boldsymbol{\sigma}^2, \boldsymbol{\Psi}^2, \mathbf{s}^2\}$

Objective: infer Θ from $\underline{\mathbf{Y}}$ using $p(\Theta \mid \underline{\mathbf{Y}}) \Rightarrow$ need for priors on the different parameters/hyperparameters involved in the model.
Parameter estimation: MCMC algorithm (Gibbs sampler) used to build estimators of the parameters of interest.

Hierarchical Bayesian model

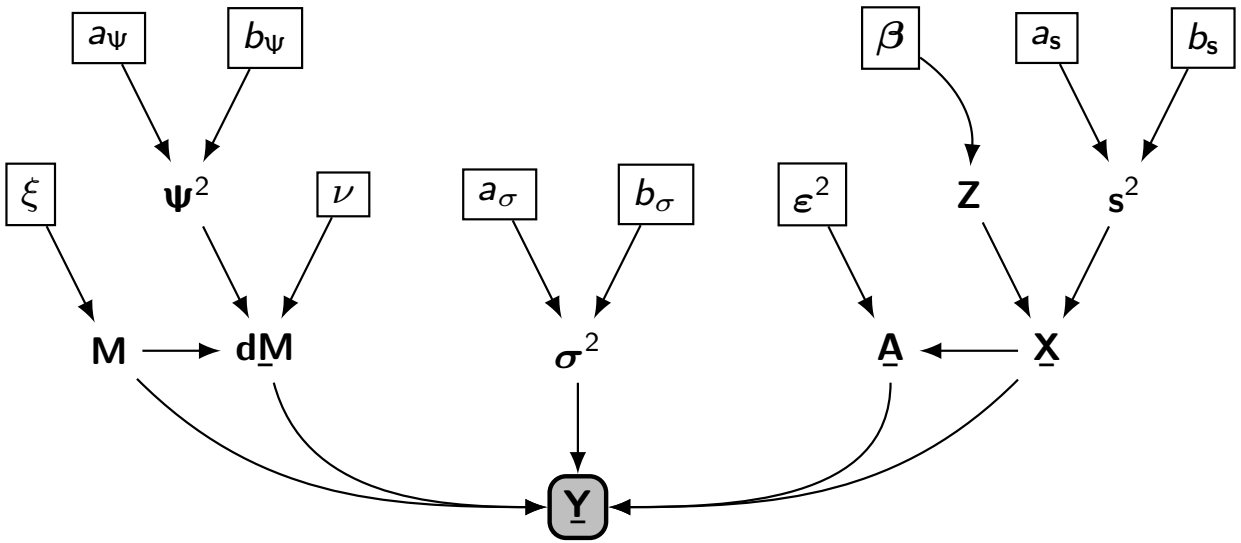

Figure 5: Description of the proposed Bayesian model using a directed acyclic graph (fixed parameters appear in boxes).

Hierachical Bayesian model: priors (I)

Abundance prior

- promotes smooth abundance variations (except when the corresponding pixel contains outliers)
- abundance sum-to-one constraint relaxed ($\mathbf{a}_{n,t}^{\mathsf{T}}\mathbf{1}_R \leq 1$) when outliers are present in the pixel (n,t) (apparition of new materials)

$$\mathbf{a}_{n,1} \mid \mathbf{x}_{n,t} = \mathbf{0}_L \sim \mathcal{U}_{\mathcal{S}_R}$$
$$\mathbf{a}_{n,t} \mid \mathbf{x}_{n,t} \neq \mathbf{0}_L \sim \mathcal{U}_{\widetilde{\mathcal{S}_R}}, \text{ for } t = 1, \ldots, T$$

$$p\left(\mathbf{a}_{n,t} \mid \mathbf{x}_{n,t} = \mathbf{0}_L, \underline{\mathbf{A}}_{\setminus\{\mathbf{a}_{n,t}\}}\right) \propto \exp\left\{-\frac{1}{2\varepsilon_n^2}\left([\mathscr{T}_{n,t}^1 \neq \emptyset]\|a_{n,t} - a_{n,\tau_{n,t}^1}\|_2^2\right)\right\}$$
$$\mathbb{1}_{\mathcal{S}_R}(\mathbf{a}_{n,t}), \text{ for } t \geq 2$$

with

$$\mathcal{S}_R = \{\mathbf{x} \in \mathbb{R}^R \mid \forall i, x_i \geq 0 \text{ and } \mathbf{x}^{\mathsf{T}}\mathbf{1}_R = 1\}$$
$$\widetilde{\mathcal{S}_R} = \{\mathbf{x} \in \mathbb{R}^R \mid \forall i, x_i \geq 0 \text{ and } \mathbf{x}^{\mathsf{T}}\mathbf{1}_R \leq 1\}$$
$$\mathscr{T}_{n,t}^1 = \{\tau < t \mid z_{n,\tau} = 0\}, \quad \tau_{n,t}^1 = \max_{\tau \in \mathscr{T}_{n,t}^1} \tau.$$

Hierachical Bayesian model: priors (II)

Outlier prior

- promotes outlier sparsity [12, 13, 14, 15, 16];
- takes advantage of possible spatial correlations between these outliers by modeling $\mathbf{z}_t \in \mathbb{R}^N$ as Ising-Markov random fields (correlations likely to occur when new materials appear).

$$p(\mathbf{x}_{n,t} \mid z_{n,t}, s_t^2) = (1 - z_{n,t})\delta(\mathbf{x}_{n,t}) + z_{n,t}\,\mathcal{N}_{\mathbb{R}_+^L}(\mathbf{0}_L, s_t^2)$$

Variability prior

- promotes smooth endmember variations from an image to another [17, 18]

$$dm_{\ell,r,1} \mid m_{\ell,r} \sim \mathcal{N}_{\mathcal{I}_{\ell,r}}(0, \nu),\ \mathcal{I}_{\ell,r} = [-m_{\ell,r}, +\infty)$$

$$dm_{\ell,r,t} | m_{\ell,r}, dm_{\ell,r,(t-1)}, \psi_{\ell,r}^2 \sim \mathcal{N}_{\mathcal{I}_{\ell,r}}\left(dm_{\ell,r,(t-1)}, \psi_{\ell,r}^2\right)$$

- ν penalizes the variability energy in the first image;
- $\psi_{\ell,r}^2$ controls the temporal evolution of the variability.

Parameter estimation

Algorithm 1: Proposed Gibbs sampler.

Input: N_{bi}, N_{MC}, $\Theta^{(0)}$, $\boldsymbol{\beta}$, ξ, a_ψ, b_ψ, $a_{\mathbf{s}}$, $b_{\mathbf{s}}$, a_σ, b_σ, ν, $\boldsymbol{\varepsilon}^2$.

for $q = 1$ **to** N_{MC} **do**

  for $(n, t) = (1, 1)$ **to** (N, T) **do**

    Draw $\mathbf{a}_{n,t}^{(q)} \sim p\left(\mathbf{a}_{n,t} \mid \mathbf{y}_{n,t}, \Theta_{\setminus\{\mathbf{a}_{n,t}\}}\right)$;

  for $r = 1$ **to** R **do**

    Draw $\mathbf{e}_r^{(q)} \sim p\left(\mathbf{e}_r \mid \underline{\mathbf{Y}}, \Theta_{\setminus\{\mathbf{e}_r\}}\right)$;

  for $t = 1$ **to** T **do**

    Draw $\mathbf{dM}_t^{(q)} \sim p\left(\mathbf{dM}_t \mid \mathbf{Y}_t, \Theta_{\setminus\{\mathbf{dM}_t\}}\right)$;

  for $(n, t) = (1, 1)$ **to** (N, T) **do**

    Draw $z_{n,t}^{(q)} \sim \mathbb{P}\left[z_{n,t} \mid \mathbf{y}_{n,t}, \Theta_{\setminus\{z_{n,t}\}}\right]$;

    Draw $\mathbf{x}_{n,t}^{(q)} \sim p\left(\mathbf{x}_{n,t} \mid \Theta_{\setminus\{\mathbf{x}_{n,t}\}}\right)$;

  for $t = 1$ **to** T **do**

    Draw $s_t^{2(q)} \sim p\left(s_t^2 \mid \Theta_{\setminus\{s_t^2\}}\right)$;

  for $t = 1$ **to** T **do**

    Draw $\sigma_t^{2(q)} \sim p\left(\sigma_t^2 \mid \Theta_{\setminus\{\sigma_t^2\}}\right)$;

  for $(\ell, r) = (1, 1)$ **to** (L, R) **do**

    Draw $\psi_{\ell,r}^{2(q)} \sim p\left(\psi_{\ell,r}^2 \mid \Theta_{\setminus\{\psi_{\ell,r}^2\}}\right)$;

Result: $\left\{\Theta^{(q)}\right\}_{q=1}^{N_{\text{MC}}}$.

Overview

Experiments on synthetic data

Data generation:

- MTHS image composed of 20 HS images of size 30×30, $L = 212$ bands, affected by smooth time-varying variability and additive white Gaussian noise;
- renders the emergence of a previously undetected material in a few pixels within specific images $\Rightarrow$ outliers.

Algorithmic setting:

- $\mathbf{X}_t^{(0)} = \mathbf{0}_{L,N}$, $\mathbf{dM}_t^{(0)} = \mathbf{0}_{L,R}$, $z_{n,t}^{(0)} = 0$, $\sigma_t^{2(0)} = 10^{-4}$, $\psi_{\ell,r}^{2(0)} = 10^{-6}$, $s_t^{2(0)} = 5 \times 10^{-3}$;
- numerical constants: $\beta_t = 1.9$, $\varepsilon_n = 10^{-4}$, $\nu = 10^{-5}$;
- $N_{\text{MC}} = 400$ M-C iterations, with $N_{\text{bi}} = 350$ burn-in iterations.

Table 1: Simulation results obtained on synthetic data (GMSE($\mathbf{A}$)$\times 10^{-2}$, GMSE($\mathbf{dM}$)$\times 10^{-3}$, RE $\times 10^{-3}$).

		aSAM($\mathbf{M}$) (°)	GMSE($\mathbf{A}$)	GMSE($\mathbf{dM}$)	RE	time (s)
$R = 3$	VCA/FCLS	14.0	1.23	/	3.20	**1**
	SISAL/FCLS	11.9	2.40	/	0.47	2
	rLMM	14.5	1.52	/	**0.04**	238
	OU	12.9	0.30	1.64	0.26	58
	Proposed (MCMC)	**8.03**	**0.17**	**0.20**	0.11	1590

Results on synthetic data (I)

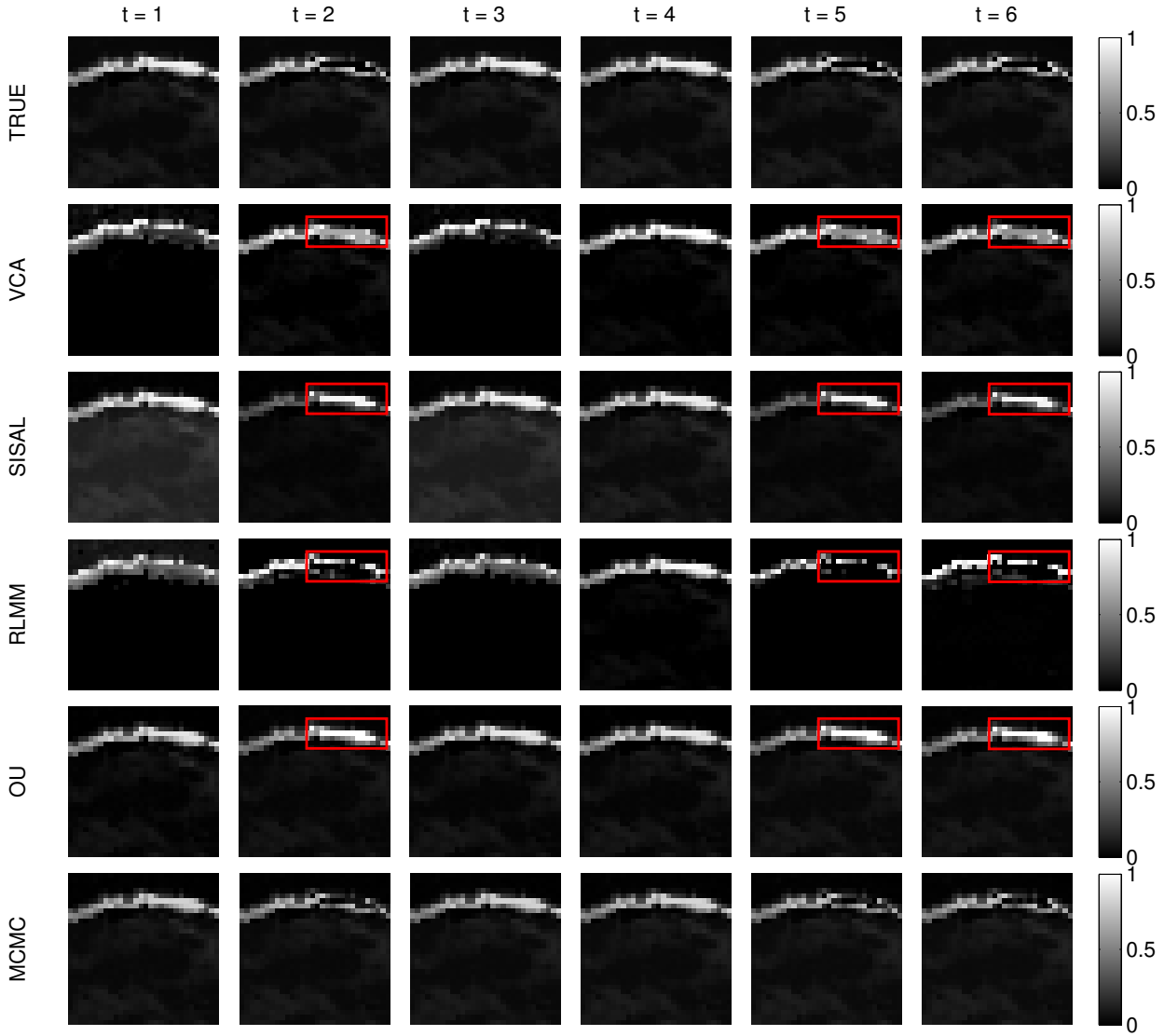

Figure 6: Abundance maps estimated for the third endmember for $t = 1$ to 6. The areas corrupted by outliers are delineated in red.

Results on synthetic data (II)

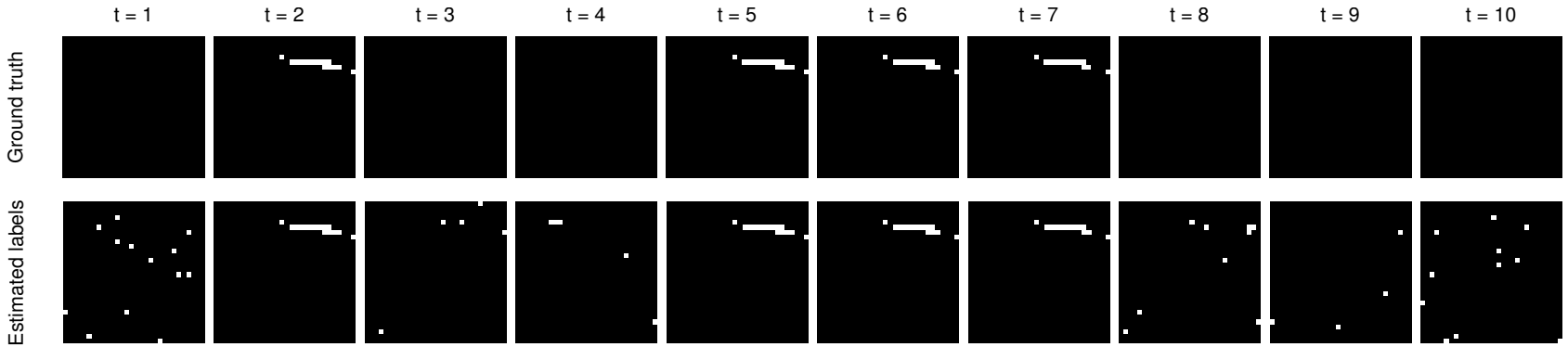

Figure 7: Ground truth (first row) and estimated labels (second row) obtained with the proposed method for $t = 1$ to 10, where each column corresponds to a time instant [0 in black, 1 in white].

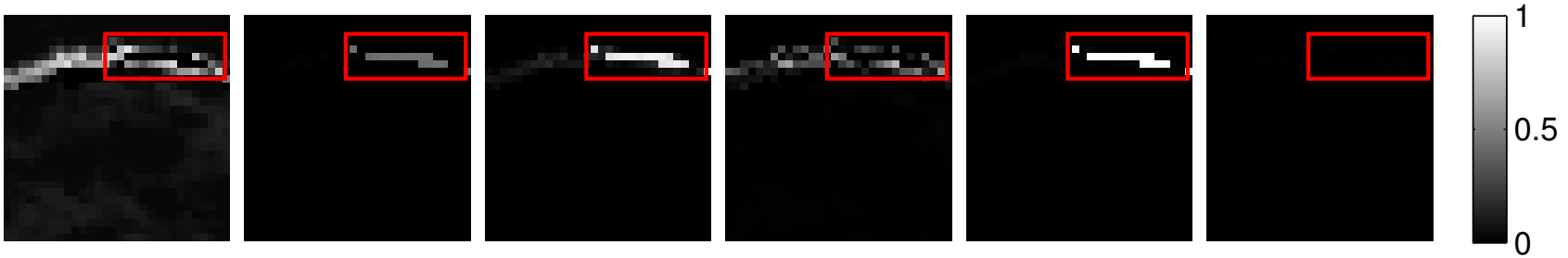

Figure 8: Map of the re-scaled abundance estimation errors for the third endmember at time $t = 2$ (from left to right: true abundances, estimation error of VCA/FCLS, SISAL/FCLS, rLMM, OU and the proposed method). Except for the proposed method, the results exhibit notable errors in pixels corrupted by outliers (area in red).

Results on synthetic data (III)

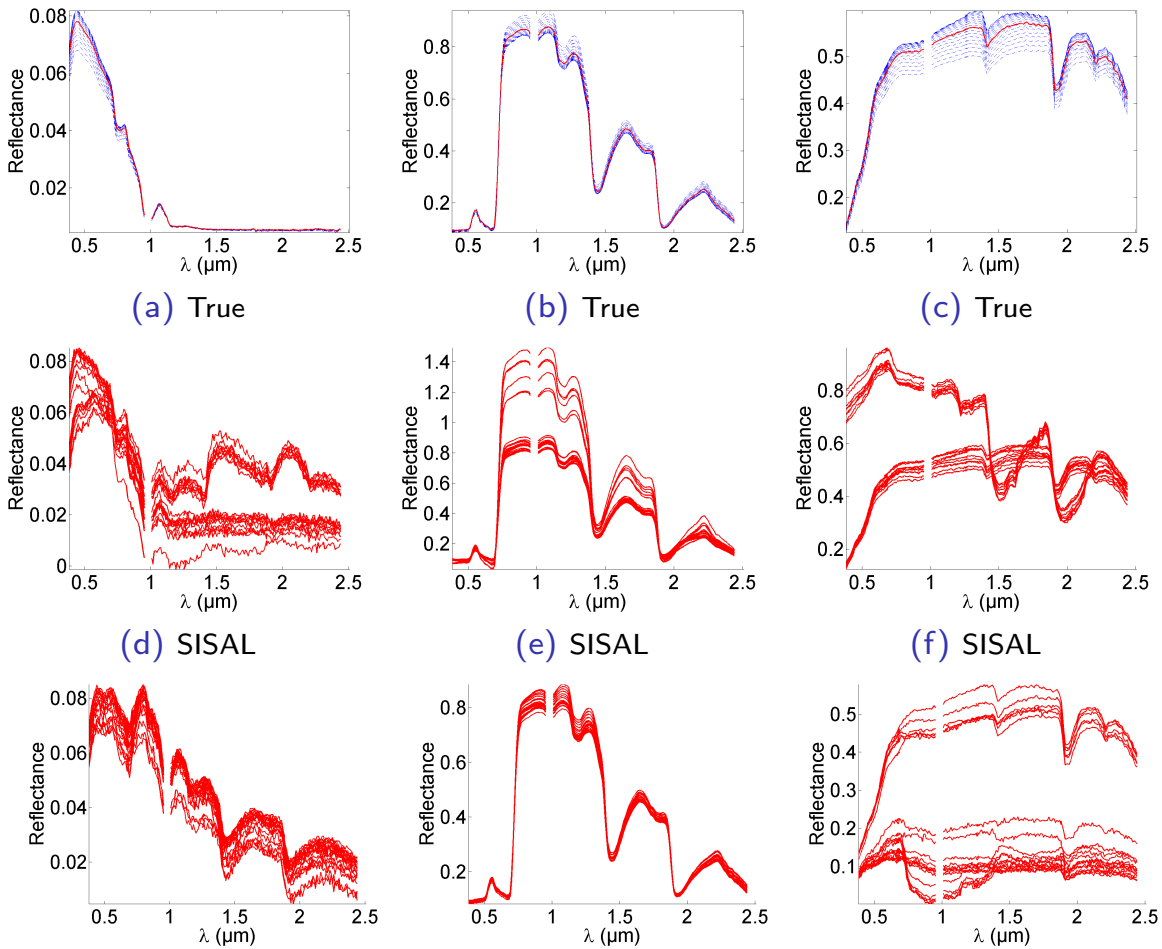

Figure 9: Endmembers (red lines) and endmember + variability (blue dotted lines) extracted from the synthetic mixture by the compared methods (in row).

Results on synthetic data (IV)

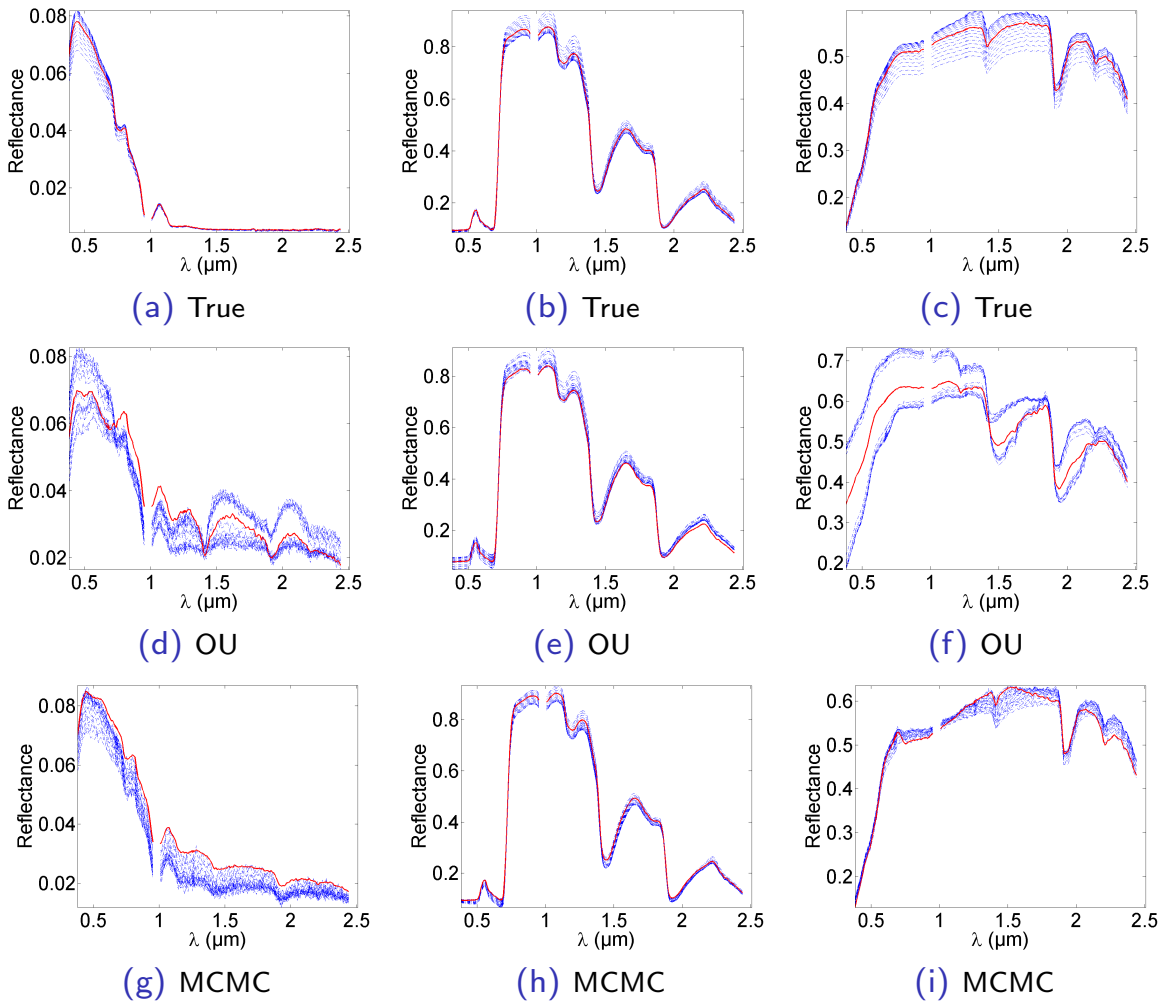

(a) True (b) True (c) True

(d) OU (e) OU (f) OU

(g) MCMC (h) MCMC (i) MCMC

Figure 10: Endmembers (red lines) and endmember + variability (blue dotted lines) extracted from the synthetic mixture by the compared methods (in row).

Overview

Conclusion and perspectives

Proposed approach

- development of an unmixing approach accounting for both smooth and abrupt spectral variations, formulated within a Bayesian framework.

Research perspectives

- ▷ application to real datasets in various contexts;
- ▷ development of unmixing algorithms scaling with the problem's dimension (e.g., distributed optimization algorithms): ongoing work;
- ▷ incorporating data from different sensors to improve unmixing results [19] (possibly relying on fusion techniques [20]).

Thank you for your attention !

Unmixing Multitemporal Hyperspectral Images Accounting for Smooth and Abrupt Variations

Pierre-Antoine Thouvenin, Nicolas Dobigeon and Jean-Yves Tourneret

University of Toulouse, IRIT/INP-ENSEEIHT

EUSIPCO 2017, Kos, Greece

September 1, 2017

Work funded by the Direction Générale de l'Armement, French Ministry of Defense.

Backup slides

- ▷ Prior assigned to the remaining parameters Priors
- ▷ Complementary results on real data Results

Priors assigned to the remaining parameters

Endmember prior

- endmembers can be *a priori* considered to live in a subspace of dimension $K \ll L$ (PCA or rPCA [21]);
- considering the decomposition used in [22] leads to

$$\mathbf{m}_r = (\mathbf{I}_L - \mathbf{U}\mathbf{U}^\mathsf{T})\bar{\mathbf{y}} + \mathbf{U}\mathbf{e}_r, \quad \mathbf{U}^\mathsf{T}\mathbf{U} = \mathbf{I}_K$$

  where $\mathbf{U}$ is a basis of the subspace and $\bar{\mathbf{y}}$ is the sample mean of $\underline{\mathbf{Y}}$;
- projected endmembers $\mathbf{e}_r$ are assigned a truncated multivariate Gaussian prior to ensure the non-negativity of $\mathbf{m}_r$

$$\mathbf{e}_r \sim \mathcal{N}_{\mathcal{E}_r}(\mathbf{0}_K, \xi\mathbf{I}_K), \text{ for } r = 1, \ldots, R. \tag{6}$$

Hyperparameter priors

- conjugate inverse-gamma priors assigned to the noise ($\boldsymbol{\sigma}^2$), the variability ($\boldsymbol{\Psi}^2$) and the outlier ($\mathbf{s}^2$) variances, i.e.,

$$\sigma_t^2 \sim \mathcal{IG}(a_\sigma, b_\sigma),\ \psi_{\ell,r}^2 \sim \mathcal{IG}(a_\Psi, b_\Psi),\ s_t^2 \sim \mathcal{IG}(a_\mathbf{s}, b_\mathbf{s}) \tag{7}$$

  where $a_\sigma = b_\sigma = a_\Psi = b_\Psi = a_\mathbf{s} = b_\mathbf{s} = 10^{-3}$.

(a) 10/04/14 (b) 02/06/14 (c) 19/09/14 (d) 17/11/14 (e) 29/04/15 (f) 13/10/15

Figure 11: Scenes used in the experiment, given with their respective acquisition date. The area delineated in red in Fig. 11e highlights a region known to contain outliers (this observation results from a previous analysis led on this dataset in [23]).

Results on real data (I)

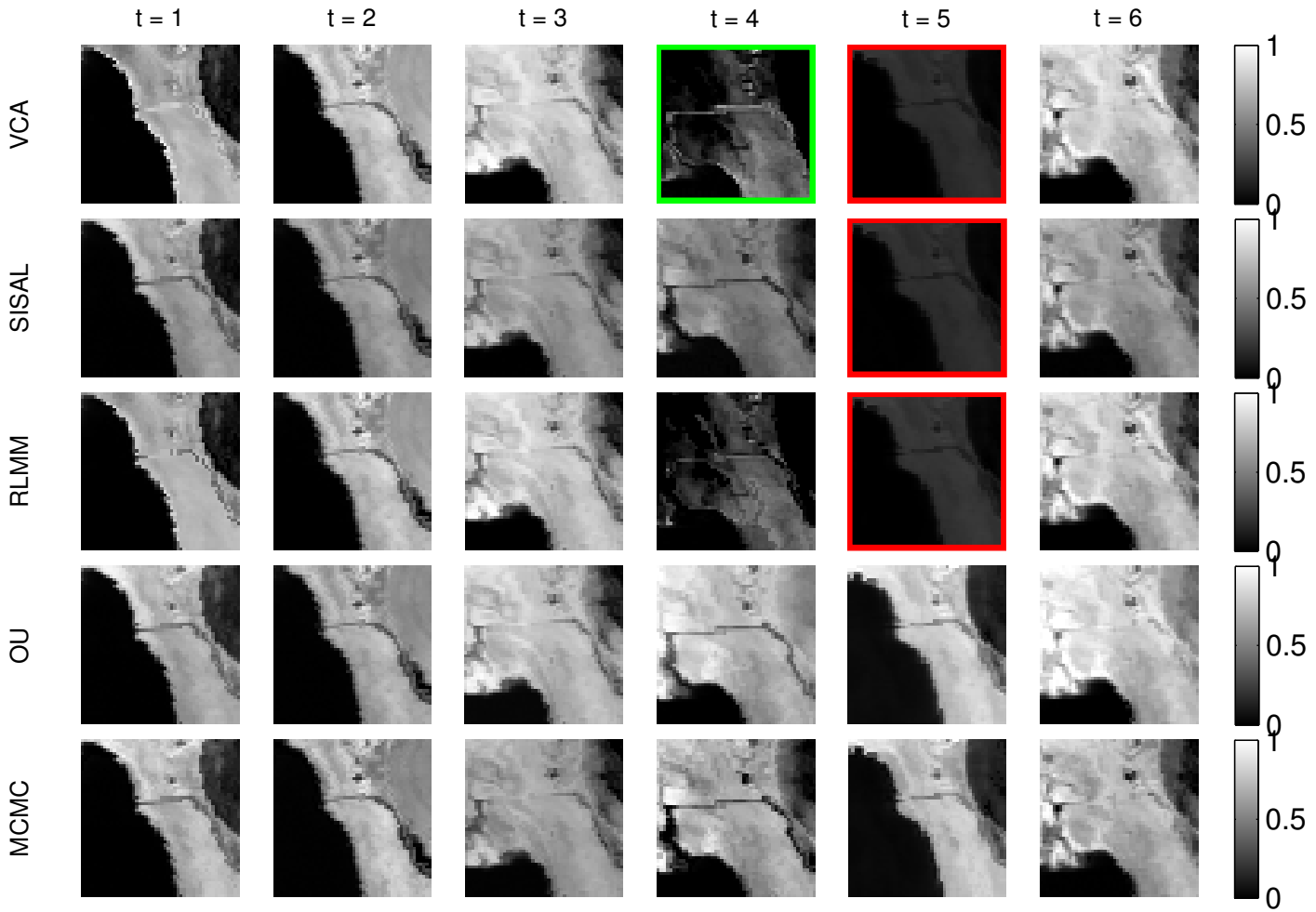

Figure 12: Soil abundance map recovered by the different methods (in row) at each time instant (in column) [VCA/FCLS, SISAL/FCLS, rLMM, OU, MCMC].

Results on real data (II)

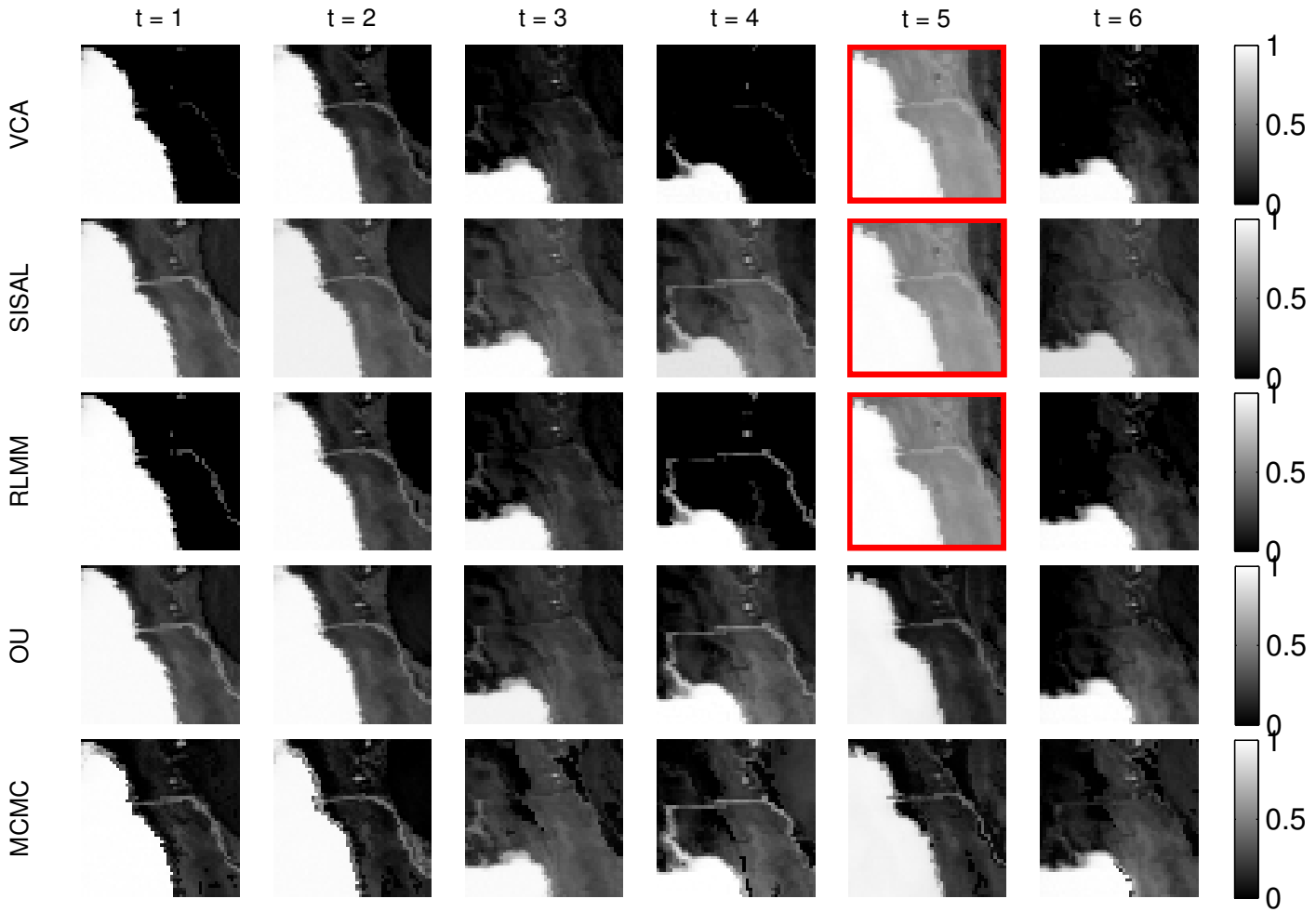

Figure 13: Water abundance map recovered by the different methods (in row) at each time instant (in column) [VCA/FCLS, SISAL/FCLS, rLMM, OU, MCMC].

Results on real data (III)

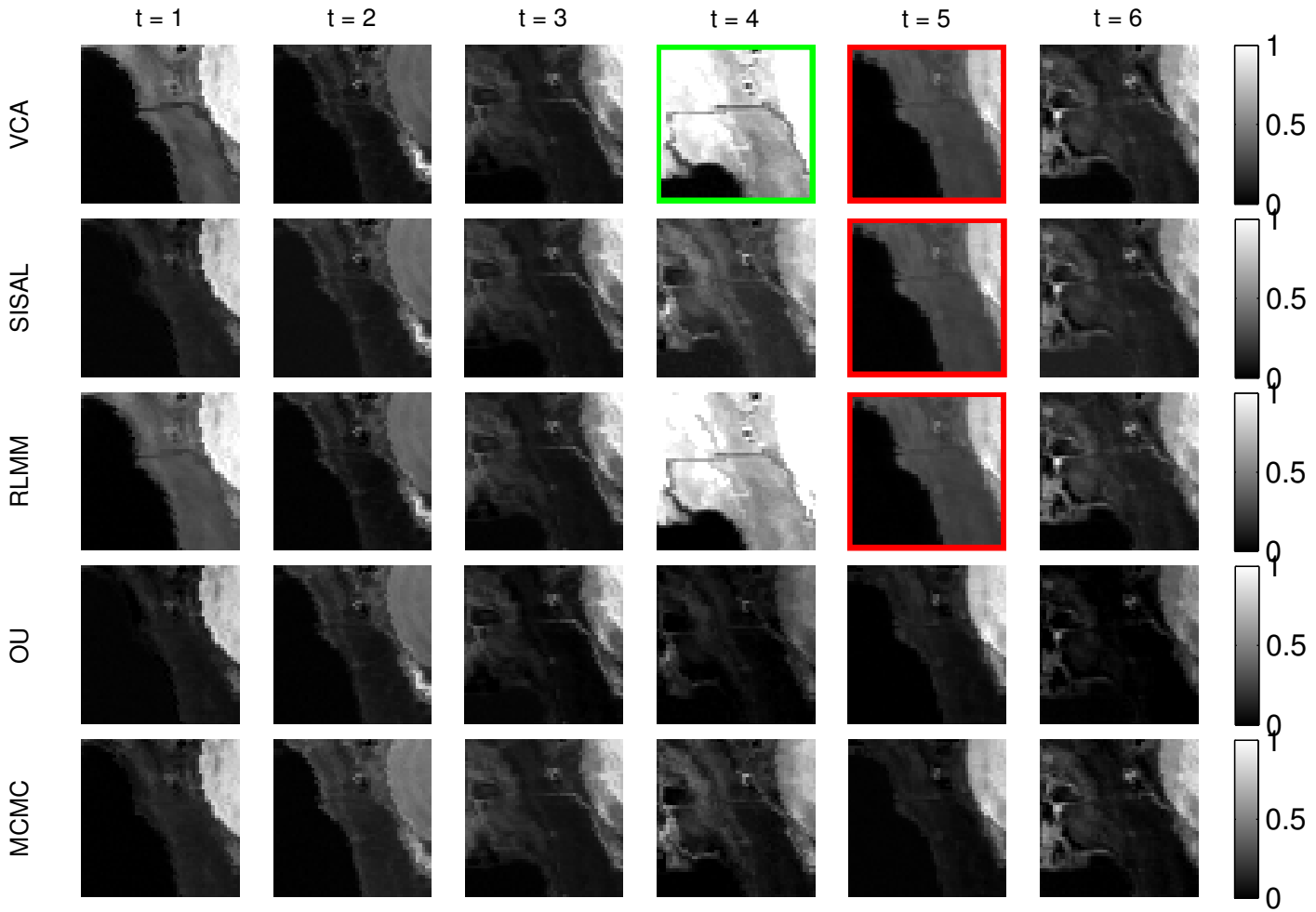

Figure 14: Vegetation abundance map recovered by the different methods (in row) at each time instant (in column) [VCA/FCLS, SISAL/FCLS, rLMM, OU, MCMC].

Results on real data (IV)

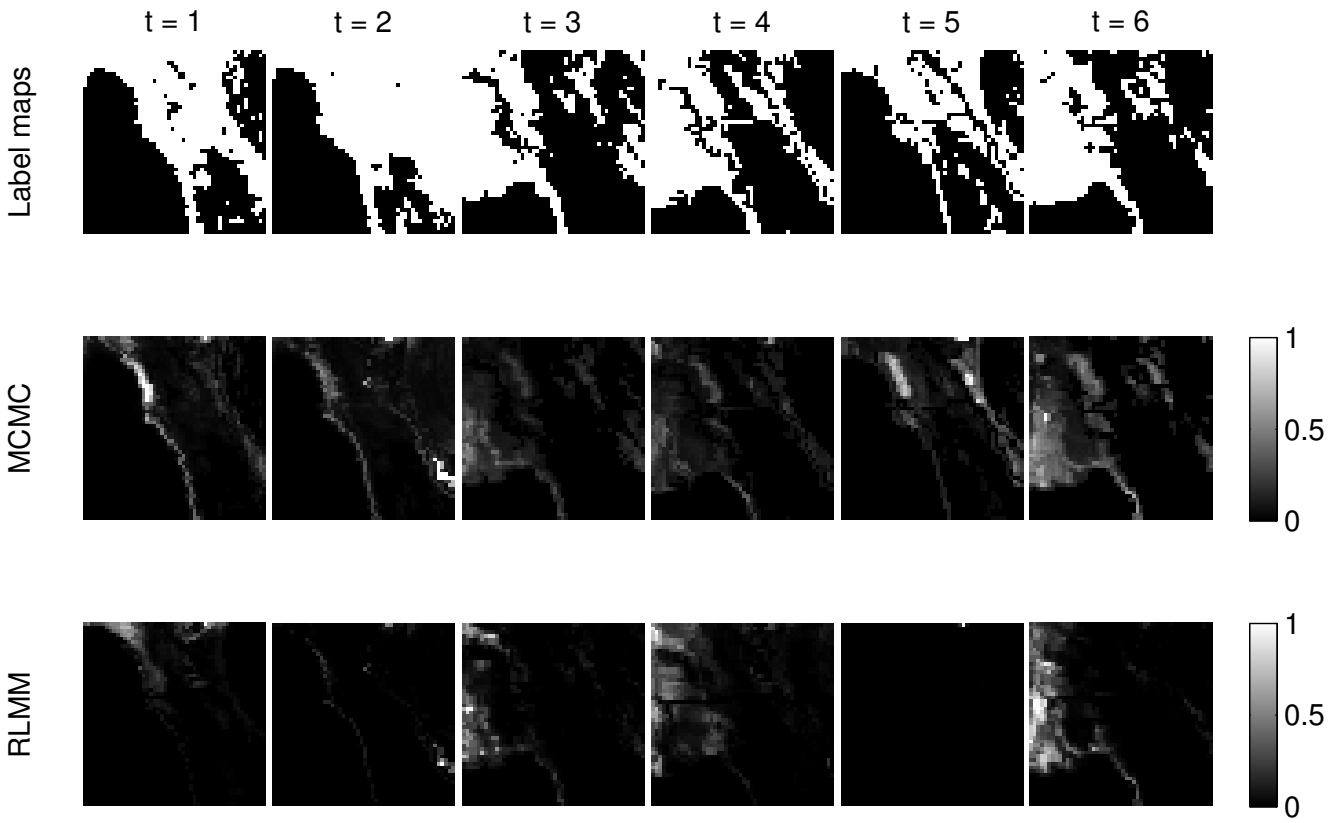

Figure 15: Outlier energy recovered by rLMM [24] and the proposed MCMC method.

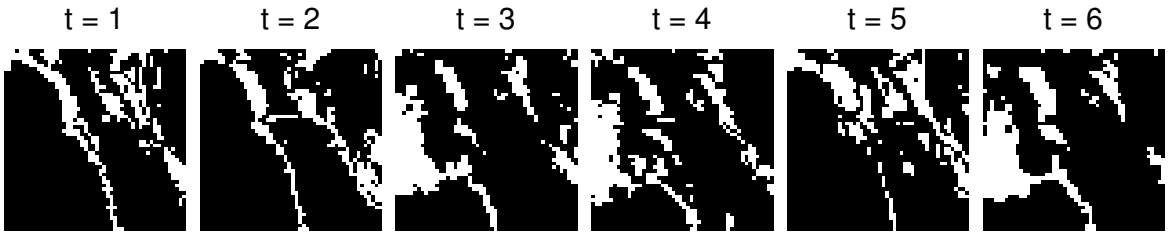

Figure 16: Non-linearity maps estimated by [25] applied to each image with the SISAL-extracted endmembers.

Results on real data (V)

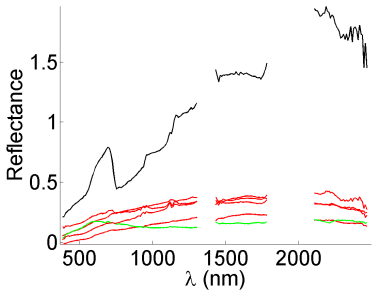

(a) Soil (VCA)

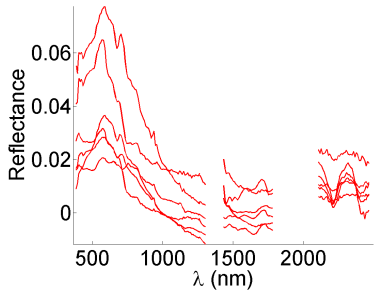

(b) Water (VCA)

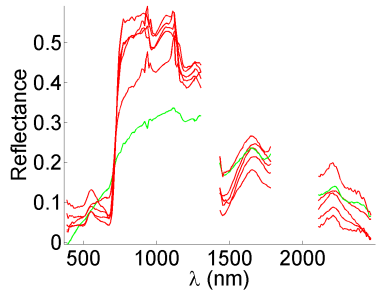

(c) Veg. (VCA)

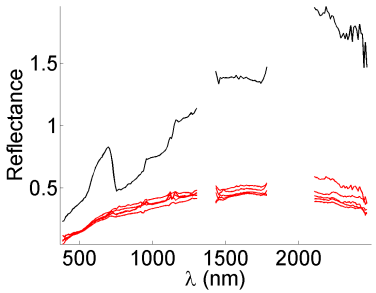

(d) Soil (SISAL)

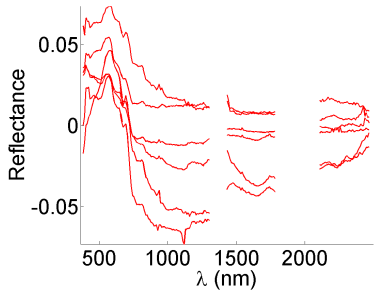

(e) Water (SISAL)

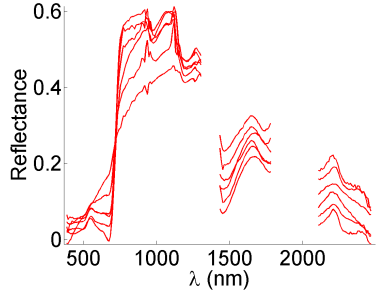

(f) Veg. (SISAL)

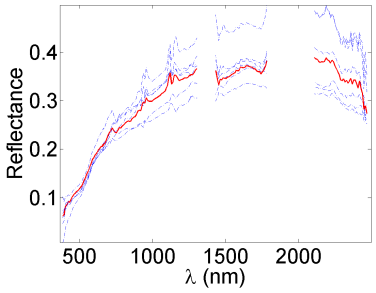

(g) MCMC

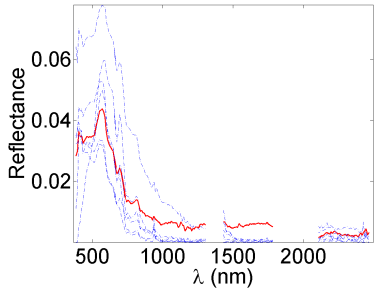

(h) MCMC

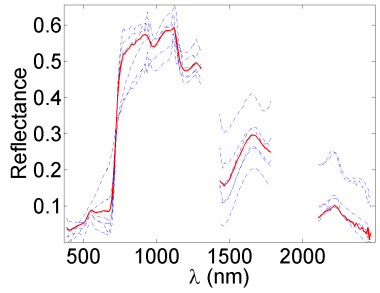

(i) MCMC

Results on real data (VI)

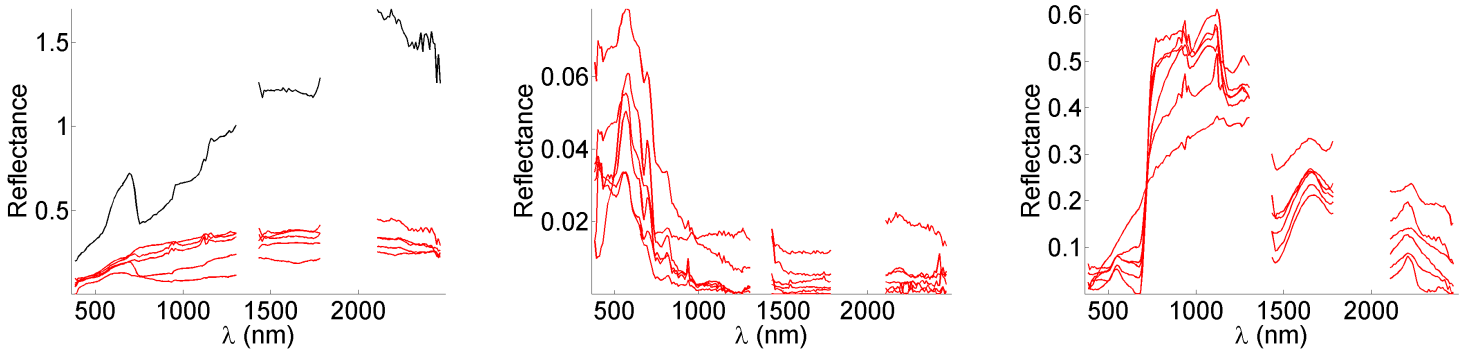

(a) Soil (rLMM) (b) Water (rLMM) (c) Veg. (rLMM)

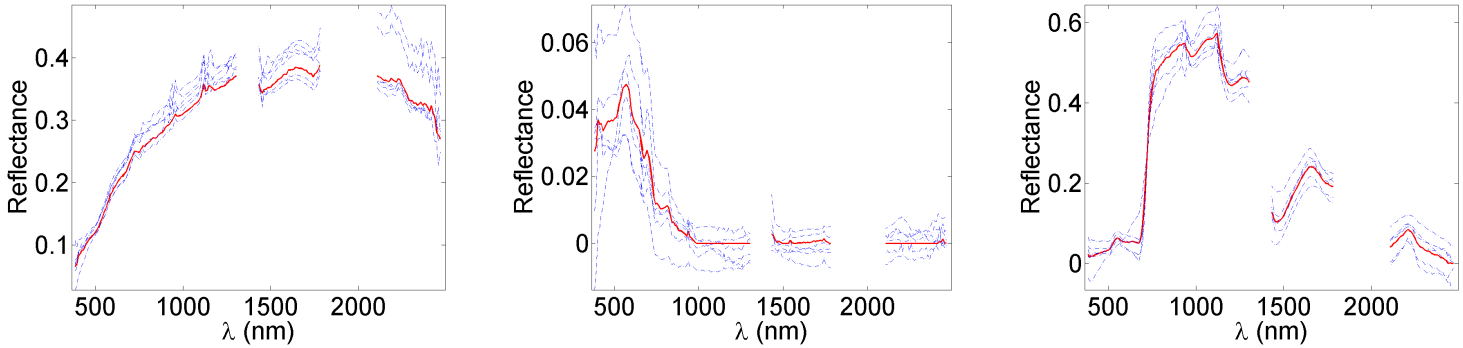

(d) Soil (OU) (e) Water (OU) (f) Veg. (OU)

Figure 18: Extracted endmembers ($\mathbf{m}_r$, red lines) and perturbed endmembers ($\mathbf{m}_r + \mathbf{dm}_{r,t}$, blue dotted lines).

Results on real data (VII)

Table 2: Simulation results on real data (RE $\times 10^{-4}$).

		RE	time (s)
$R = 3$	VCA/FCLS	11.73	**1**
	SISAL/FCLS	2.38	2
	rLMM	0.66	106
	OU	2.08	26
	Proposed	**0.19**	3700

[1] J. M. Bioucas-Dias, A. Plaza, N. Dobigeon, M. Parente, Q. Du, P. Gader, and J. Chanussot, "Hyperspectral unmixing overview: Geometrical, statistical, and sparse regression-based approaches," *IEEE J. Sel. Topics Appl. Earth Observ. in Remote Sens.*, vol. 5, no. 2, pp. 354–379, Apr. 2012.

[2] A. Halimi, Y. Altmann, N. Dobigeon, and J.-Y. Tourneret, "Nonlinear unmixing of hyperspectral images using a generalized bilinear model," *IEEE Trans. Geosci. Remote Sens.*, vol. 49, no. 11, pp. 4153–4162, Nov. 2011.

[3] N. Dobigeon, J.-Y. Tourneret, C. Richard, J. C. M. Bermudez, S. McLaughlin, and A. O. Hero, "Nonlinear unmixing of hyperspectral images: Models and algorithms," *IEEE Signal Process. Mag.*, vol. 31, no. 1, pp. 89–94, Jan. 2014.

[4] R. Heylen, M. Parente, and P. Gader, "A review of nonlinear hyperspectral unmixing methods," *IEEE J. Sel. Topics Appl. Earth Observ. in Remote Sens.*, vol. 7, no. 6, pp. 1844–1868, Jun. 2014.

[5] Y. Altmann, N. Dobigeon, and J.-Y. Tourneret, "Unsupervised post-nonlinear unmixing of hyperspectral images using a Hamiltonian Monte Carlo algorithm," *IEEE Trans. Image Process.*, vol. 23, no. 6, pp. 2663–2675, Jun. 2014.

[6] B. Somers, M. Zortea, A. Plaza, and G. Asner, "Automated extraction of image-based endmember bundles for improved spectral unmixing," *IEEE J. Sel. Topics Appl. Earth Observ. in Remote Sens.*, vol. 5, no. 2, pp. 396–408, Apr. 2012.

[7] D. Roberts, M. Gardner, R. Church, S. Ustin, G. Scheer, and R. Green, "Mapping chaparral in the Santa Monica mountain using multiple endmember spectral mixture models," *Remote Sens. Environment*, vol. 65, no. 3, pp. 267–279, Sep. 1998.

[8] M. A. Goenaga, M. C. Torres-Madronero, M. Velez-Reyez, S. J. V. Bloem, and J. D. Chinea, "Unmixing analysis of a time series of hyperion images over the Guánica dry forest in Puerto Rico," *IEEE J. Sel. Topics Appl. Earth Observ. in Remote Sens.*, vol. 6, no. 2, pp. 329–338, Apr. 2013.

[9] O. Eches, N. Dobigeon, C. Mailhes, and J.-Y. Tourneret, "Bayesian estimation of linear mixtures using the normal compositional model. Application to hyperspectral imagery," *IEEE Trans. Image Process.*, vol. 19, no. 6, pp. 1403–1413, Jun. 2010.

[10] A. Halimi, N. Dobigeon, and J.-Y. Tourneret, "Unsupervised unmixing of hyperspectral images accounting for endmember variability," *IEEE Trans. Image Process.*, vol. 24, no. 12, pp. 4904–4917, Dec. 2015.

[11] X. Du, A. Zare, P. Gader, and D. Dranishnikov, "Spatial and spectral unmixing using the beta compositional model," *IEEE J. Sel. Topics Appl. Earth Observ. in Remote Sens.*, vol. 7, no. 6, pp. 1994–2003, Jun. 2014.

[12] J. J. Kormylo and J. M. Mendel, "Maximum likelihood detection and estimation of Bernoulli-Gaussian processes," *IEEE Trans. Inf. Theory*, vol. 28, no. 3, pp. 482–488, May 1982.

[13] M. Lavielle, "Bayesian deconvolution of Bernoulli-Gaussian processes," *Signal Process.*, vol. 33, no. 1, pp. 67–79, Jul. 1993.

[14] S. Bourguignon and H. Carfantan, "Bernoulli-Gaussian spectral analysis of unevenly spaced astrophysical data," in *Proc. IEEE-SP Workshop Stat. and Signal Processing (SSP)*, Bordeaux, France, Jul. 2005, pp. 811–816.

[15] C. Bazot, N. Dobigeon, and J.-Y. Tourneret, "Bernoulli-Gaussian model for gene expression analysis," in *Proc. IEEE Int. Conf. Acoust., Speech, and Signal Processing (ICASSP)*, Prague, Czech Republic, May 2011, pp. 5996–5999.

[16] J. P. Vila and P. Schniter, "Expectation-Maximization Gaussian-mixture approximate message passing," *IEEE Trans. Signal Process.*, vol. 61, no. 19, pp. 4658–4672, Oct. 2013.

[17] A. Halimi, N. Dobigeon, J.-Y. Tourneret, S. McLaughlin, and P. Honeine, "Unmixing hyperspectral images accounting for temporal and spatial endmember variability," in *Proc. European Signal Process. Conf. (EUSIPCO)*, Nice, France, Sep. 2015, pp. 1686–1690.

[18] S. Henrot, J. Chanussot, and C. Jutten, "Dynamical spectral unmixing of multitemporal hyperspectral images," *IEEE Trans. Image Process.*, vol. 25, no. 7, pp. 3219–3232, Jul. 2016.

[19] N. Yokoya, X. X. Zhu, and A. Plaza, "Multisensor Coupled Spectral Unmixing for Time-Series Analysis," *IEEE Trans. Geosci. Remote Sens.*, vol. 55, no. 5, pp. 2842–2857, May 2017.

[20] Q. Wei, J. M. Bioucas-Dias, N. Dobigeon, J.-Y. Tourneret, M. Chen, and S. Godsill, "Multi-band image fusion based on spectral unmixing," *IEEE Trans. Geosci. Remote Sens.*, vol. 2, no. 4, pp. 7236–7249, Dec. 2016.

[21] E. J. Candès, X. Li, Y. Ma, and J. Wright, "Robust principal component analysis?" *journal of ACM*, vol. 58, no. 1, pp. 1–37, 2009.

[22] N. Dobigeon, S. Moussaoui, M. Coulon, J.-Y. Tourneret, and A. O. Hero, "Joint Bayesian endmember extraction and linear unmixing for hyperspectral imagery," *IEEE Trans. Signal Process.*, vol. 57, no. 11, pp. 4355–4368, Nov. 2009.

[23] P.-A. Thouvenin, N. Dobigeon, and J.-Y. Tourneret, "Online unmixing of multitemporal hyperspectral images accounting for spectral variability," *IEEE Trans. Image Process.*, vol. 25, no. 9, pp. 3979–3990, Sep. 2016.

[24] C. Févotte and N. Dobigeon, "Nonlinear hyperspectral unmixing with robust nonnegative matrix factorization," *IEEE Trans. Image Process.*, vol. 24, no. 12, pp. 4904–4917, Dec. 2015.

[25] Y. Altmann, N. Dobigeon, J.-Y. Tourneret, and J. C. M. Bermudez, "A robust test for nonlinear mixture detection in hyperspectral images," in *Proc. IEEE Int. Conf. Acoust., Speech, and Signal Processing (ICASSP)*, Vancouver, Canada, Jun. 2013, pp. 2149–2153.